THE JOURNAL OF BIOLOGICAL CHEMISTRY VOL. 288, NO. 50, pp. 35840–35851, December 13, 2013
Published in the U.S.A.

Structural Insights of tBid, the Caspase-8-activated Bid, and Its BH_3 Domain*

Received for publication, July 19, 2013, and in revised form, October 18, 2013 Published, JBC Papers in Press, October 24, 2013, DOI 10.1074/jbc.M113.503680

Yu Wang and Nico Tjandra[1]

From the Laboratory of Molecular Biophysics, Biochemistry and Biophysics Center, NHLBI, National Institutes of Health, Bethesda, Maryland 20892

Background: The membrane-associated tBid promotes Bax membrane insertion and activation.
Results: tBid adopts an extended structure in 1-palmitoyl-2-hydroxy-*sn*-glycero-3-[phospho-RAC-(1-glycerol)] (LPPG) micelles with its six helices including the BH_3 domain interacting with the micelles.
Conclusion: An "on the membrane" binding mode was suggested for tBid interaction with Bax.
Significance: Revealing tBid structure on the membrane is key to the understanding of tBid-mediated Bax activation.

The Bcl-2 family proteins regulate mitochondria-mediated apoptosis through intricate molecular mechanisms. One of the pro-apoptotic proteins, tBid, can induce apoptosis by promoting Bax activation, Bax homo-oligomerization, and mitochondrial outer membrane permeabilization. Association of tBid on the mitochondrial outer membrane is key to its biological function. Therefore knowing the conformation of tBid on the membrane will be the first step toward understanding its crucial role in triggering apoptosis. Here, we present NMR characterization of the structure and dynamics of human tBid in 1-palmitoyl-2-hydroxy-*sn*-glycero-3-[phospho-RAC-(1-glycerol)] micelles. Our data showed that tBid is monomeric with six well defined α-helices in the micelles. Compared with the full-length Bid structure, a longer flexible loop between tBid helix α_4 and α_5 was observed. Helices in tBid do not pack into a compact-fold but form an extended structure with a C-shape configuration in the micelles. All six tBid helices were shown to interact with LPPG micelles, with helix α_6 and α_7 being more embedded. Of note, the BH_3-containing helix α_3, which was previously believed to be exposed above the membrane surface, is also membrane associated, suggesting an "on the membrane" binding mode for tBid interaction with Bax. Our data provided structural details on the membrane-associated state of tBid and the functional implications of its membrane-associated BH_3 domain.

Apoptosis (programmed cell death) plays an important role in tissue development and maintenance (1). A group of apoptosis regulator proteins, the Bcl-2 (B-cell lymphoma 2) family proteins, were discovered to work coordinately to modulate mitochondrial outer membrane permeabilization (MOMP)[2] (2–4). Bcl-2 family members share at least one of four BH (Bcl-2 homology) domains and many of them possess a transmembrane domain at the C terminus. Based on their apoptotic function, Bcl-2 family proteins are classified into two groups: pro-apoptotic and anti-apoptotic proteins. A subgroup of the pro-apoptotic proteins, containing only the BH_3 domain (*e.g.* Bid, Bim, and PUMA), can directly interact with pro-apoptotic proteins Bax/Bak and promote their homo-oligomerization on the membrane and lead to MOMP (5–7). This represents the major process of the direct activation model for apoptosis initiation. Another competing model, the indirect activation (or displacement) model, suggests anti-apoptotic proteins (*e.g.* Bcl-2, Bcl-xL, Bcl-w, and Mcl-1) can heterodimerize with Bax/Bak to suppress their pro-apoptotic activity (8). Within this model, a sensitizing role was implied for the BH_3-only proteins (*e.g.* Bad), which can bind anti-apoptotic proteins, displace Bax/Bak, and indirectly promote Bax/Bak oligomerization and MOMP (9–16). Cumulative evidences imply mitochondrial membrane insertion of many Bcl-2 family proteins is critical for their apoptotic functions and the translocation from cytosol to mitochondrial membrane could account for totally different inter-protein interactions among Bcl-2 family members (13, 17, 18). To accommodate such effects in the context of membrane association, the "embedded together" model was proposed with the recognition that final steps of Bax/Bak activation and MOMP take place on the membrane (13). Currently, little structural information is available on the membrane-associated state of Bcl-2 family proteins compared with their well studied cytosolic forms (19).

The BH_3-only protein, Bid, was shown to bridge the cross-talk between extrinsic and intrinsic pathways of apoptosis through its cleavage by caspase-8 (20–22), a downstream mediator of Fas or the tumor necrosis factor (TNF) death receptor signaling pathway (23, 24). The proteolytic cleavage of cytosolic Bid by activated caspase-8 results in two fragments: p_7 (7 kDa) and p_{15} (15 kDa) (21, 25). After cleavage, the C-terminal fragment (p_{15}), also known as tBid (truncated Bid), translocates to the mitochondrial outer membrane (21). The membrane asso-

* This work was supported, in whole or in part, by a National Institutes of Health grant from the Intramural Research Program of the NHLBI (to N. T.).
The atomic coordinates and structure factors (code 2M5I) have been deposited in the Protein Data Bank (http://wwpdb.org/).
The chemical shifts can be accessed through the Biological Magnetic Resonance Bank (BMRB) under BMRB accession number 19054.
[1] To whom correspondence should be addressed. Tel.: 301-402-3029; Fax: 301-402-3405; E-mail: tjandran@nhlbi.nih.gov.
[2] The abbreviations used are: MOMP, mitochondrial outer membrane permeabilization; tBid, truncated Bid; LPPG, 1-palmitoyl-2-hydroxy-*sn*-glycero-3-[phospho-RAC-(1-glycerol)]; PRE, paramagnetic relaxation enhancement; TEV, tobacco etch virus; HSQC, heteronuclear single quantum coherence; r.m.s., root mean square.

ciation of tBid was shown to be important for the efficient recruitment of cytosolic Bax to the mitochondrial outer membrane (18, 26). Through interaction with the tBid BH_3 domain, Bax was suggested to undergo conformational changes, membrane insertion, and homo-oligomerization at the mitochondrial outer membrane, mediating MOMP and cytochrome *c* release (17, 18, 26–28). However, studies also suggested tBid could bypass Bax/Bak and directly promote the mitochondrial permeabilization by tBid alone with the induction of the negative membrane curvature (29–31).

In the cytosol, both human and mouse Bid contain eight α-helices with two hydrophobic helices (helix α_6 and α_7) forming the core of the protein (32, 33). After caspase-8 cleavage, the Bid N-terminal p_7 fragment retains tight association with tBid through primarily hydrophobic interactions (32). Earlier studies suggested that tBid dissociated from the p_7 fragment upon contact with the hydrophobic membrane and exposed its hydrophobic p_7 binding pocket, promoting tBid to undergo conformational changes on the membrane (34–36). *In vitro*, isolated tBid was shown to bind to membranes quickly and is competent to activate Bax-mediated membrane permeabilization (18). A previous solid-state NMR study suggested that tBid associated with the membrane with an orientation parallel to the membrane surface and without membrane-traversing helix insertion (37). Additionally, membrane-associated tBid showed helical propensity at Bid helices α_{6-8} regions with helix α_6 tilted into the membrane based on the EPR studies (34). However, these studies did not provide specific information on tBid helical boundaries, the tertiary-fold of tBid, and its overall interaction with the membrane. Currently, a proposed model indicated that tBid helices α_{6-8} are membrane associated, leaving the tBid BH_3 domain fully exposed above the membrane surface for potential interactions with other proteins (35). This model is useful to explain some of the observed tBid functional data in solution but provided limited information regarding tBid function on the membrane (35). The exposed conformation of tBid BH_3 domain above the membrane surface is energetically unfavorable unless stabilized by other proteins. It is inconsistent with the finding that the tBid BH_3 domain peptide was membrane associated and fully competent to activate Bax (38). Thus, it is still not clear whether the tBid BH_3 domain forms a helix on the membrane and whether its hydrophobic residues that were believed to be involved in the protein interactions in solution behave differently on the membrane by interacting with the membrane instead (20).

To address these questions with more structural details, we chose to determine the full-length tBid structure on the membrane along with the characterization of tBid regions that are interacting with the membrane. Here, we used solution NMR methods to characterize human tBid in membrane mimic 1-palmitoyl-2-hydroxy-*sn*-glycero-3-[phospho-RAC-(1-glycerol)] (LPPG) micelles. Our data showed tBid preserved all six Bid helices (α_3 to α_8), including the BH_3-containing helix α_3. Compared to full-length Bid, the biggest difference was observed for tBid helix α_5, which is a shorter helix with a longer flexible loop connecting it to helix α_4. tBid possessed a C-shape conformation with a close but no direct contact between N and C termini of tBid in LPPG micelles as evidenced by paramagnetic relaxation enhancement (PRE) measurements. Furthermore, extensive interactions with LPPG micelles were observed for all six tBid helices. Specifically, the BH_3-containing helix α_3, which was previously believed to be exposed outside the membrane, is also membrane associated. The protein-micelle interaction and protein backbone dynamics data suggested helices α_6 and α_7 are likely to be more embedded into the micelles than the rest of the helices. Our findings provide detailed structural information of membrane-associated tBid and suggest the membrane-associated feature of tBid BH_3 domain favors an "on the membrane" binding mode with Bax.

EXPERIMENTAL PROCEDURES

Cloning and Sample Preparation—The pET15b-Bid^{FL} vector carrying human Bid cDNA was used to produce full-length Bid protein. To produce tBid in a more efficient manner without caspase-8 cleavage, we replaced the caspase-8 cleavage site with a TEV protease cleavage site by mutating the pET15b-Bid^{FL} vector (^{53}YDELQTDG to ^{53}DENLYFQG). Thus the modified full-length Bid can be cleaved by TEV protease and the resulting cleavage product tBid will be the same as the native tBid. The modified plasmid (pET15b-Bid^{TEV}) was transformed into *Escherichia coli* BL21(DE3) cells to express recombinant protein. Isotopically (^{15}N or ^{15}N,^{13}C) labeled proteins were produced in isotope-enriched M9 minimal media. The perdeuterated tBid sample was grown in 99% D_2O minimal media. The *E. coli* cells were grown at 37 °C, induced with 1 mM isopropyl 1-thio-β-D-galactopyranoside at A_{600} ~0.8, and cell growth was continued overnight at 18 °C. The cells were harvested by centrifugation, resuspended in lysis buffer (20 mM Tris-HCl, pH 8.0, 500 mM NaCl, 5 mM imidazole, 1 mM PMSF), and sonicated. The lysate was centrifuged at 34,000 × *g* for 30 min at 4 °C and the supernatant was loaded to Ni^{2+} affinity chromatography. The His_6-tagged full-length Bid^{TEV} was eluted using elution buffer (20 mM Tris-HCl, pH 8.0, 500 mM NaCl, 250 mM imidazole) and dialyzed into buffer A (20 mM Tris-HCl, pH 8.0) before it was further purified by an ion-exchange chromatography on a HiTrap 1-ml Q column (GE Healthcare) with a linear salt gradient. The purified full-length Bid^{TEV} was pooled and mixed with 200 units of AcTEV protease (Invitrogen) for cleavage by dialyzing against 1 liter of TEV cleavage buffer (50 mM Tris-HCl, pH 8.0, 0.5 mM EDTA, 1.0 mM DTT) overnight at room temperature. The cleaved protein mixture was loaded onto the Ni^{2+} affinity chromatography and tBid was separated by washing with lysis buffer with 1.2% (w/v) *n*-octyl-β-D-glucoside. The fraction containing purified tBid was collected and dialyzed against buffer (20 mM Tris-HCl, 100 mM NaCl, pH 8.0) to remove detergent *n*-octyl-β-D-glucoside. After dialysis, tBid precipitated out of solution and was collected by centrifugation. The NMR sample of tBid at 0.5–1.0 mM was prepared by dissolving the protein pellet into NMR buffer (50 mM potassium phosphate, pH 6.6) supplemented with 8% (160 mM) LPPG, 10% D_2O, and 0.02% sodium azide. The tBid samples in LPPG micelles were kept at 45 °C at all times for better sample stability.

NMR Spectroscopy—All NMR measurements were carried out on a Bruker Avance 600 MHz spectrometer with a room temperature probe, or a Bruker Avance 800 MHz or a Bruker

Avance 900 MHz spectrometer with cryogenic probes. The following experiments were used for backbone resonances assignments: three-dimensional HNCA (39), CBCA(CO)NH (40), HNCACB (41), HBHA(CO)NH (42), and HNCO (43). Three-dimensional ^{15}N-edited NOESY-HSQC (t_{mix} = 70 ms) (42) and four-dimensional ^{13}C/^{13}C-edited NOESY (t_{mix} = 70 ms) (44) experiments were acquired for inter-proton NOE distance restraints. The backbone ^{15}N T_1 measurement obtained using a 800 MHz spectrometer was recorded at various delays: 8, 120, 320, 600, 880, 1200, 1600, and 2240 ms (45). For 600 MHz, T_1 delays used were 8.0, 128, 384, 560, 800, 1040, 1280, and 1600 ms. The ^{15}N T_2 measurement obtaining using a 800 MHz spectrometer was carried out using a Carr-Purcell-Meiboom-Gill pulse sequence at various total delays: 4.0, 12, 24, 36, 48, 68, 88, and 128 ms (45). For 600 MHz, T_2 delays used were 8.0, 24, 40, 56, 72, 100, 132, and 192 ms. The PRE ^1H_N-Γ_2 rates were determined from a two-time point (0.04 and 12 ms) interleaved measurement using a TROSY-based experiment (46). The protein backbone ^{15}N relaxation dispersion experiments were carried out using two different τ_{cp} of 0.3 and 6 ms in the CPMG refocusing element with a constant delay time of 48 ms. All NMR data were processed using NMRPipe (47) and analyzed with NMRview (48) and PIPP (49). Experimental errors were estimated based on the spectral noise as described previously (50).

Characterization of Protein-Micelle Interaction—A ^{15}N-labeled perdeuterated tBid sample was expressed in M_9 minimal media supplemented with 99.9% D_2O and ^{15}N ammonium chloride. The three-dimensional ^{15}N-edited NOESY-HSQC (t_{mix} = 70 ms) experiment was acquired to obtain the NOE distance information between the protein backbone amide protons (H^N) and the LPPG protons.

Site-directed Mutagenesis—tBid single cysteine mutants (S78C, Q136C, and Q180C) were prepared using a QuikChange site-directed mutagenesis kit (Stratagene). These point mutations were introduced using pET15b-Bid^{TEV} expressing plasmid as template. All mutants were confirmed by DNA sequencing.

Paramagnetic Relaxation Enhancement—Because there is no cysteine in tBid, non-native cysteines were introduced by site-directed mutagenesis at the respective sites mentioned above. The full-length Bid bearing the cysteine mutant was first expressed, purified, and cleaved as described above. After TEV cleavage, the protein sample was soaked with DTT at a final concentration of 20 mM to reduce any possible cysteine disulfide bonds. The protein was then exchanged into a reaction buffer (100 mM Tris-HCl, 1 mM diethylenetriaminepentaacetic acid, pH 8.5) using a PD-10 desalting column. Following that, parallel spin probe labeling reactions were carried out by mixing the protein sample with 20× molar excess of the paramagnetic probe MTSL (1-oxyl-2,2,5,5-tetramethyl-η3-pyrroline-3-methyl) methanethiosulfonate (Toronto Research Chemicals Inc.) or diamagnetic analog dMTSL (1-acetyl-2,2,5,5-tetramethyl-η3-pyrroline-3-methyl)methanethiosulfonate (Toronto Research Chemicals Inc.) at room temperature overnight. The stock of both MTSL and dMTSL reagents had been previously dissolved at 20 mg/ml in acetonitrile. After the reactions, excess spin label was removed by dialysis against a buffer (20 mM Tris-HCl, 100 mM NaCl, pH 8.0). Both the paramagnetic and diamagnetic protein samples were further purified in 1.2% *n*-octyl-β-D-glucoside as described above. Experimental errors for the PRE were estimated as previously described (51). Labeling of the tBid samples was confirmed by liquid chromatography/mass spectrometry. A two-dimensional ^{1}H,^{15}N-HSQC spectrum of each paramagnetic tBid sample was recorded and no obvious chemical shift changes observed, indicating spin labeling did not disrupt tBid structure. Solvent PRE experiments were performed by stepwise addition of the water-soluble spin label reagent gadodiamide (aqua[5,8-bid(carboxymethyl)-11-[2-(methylamino)-2-oxoethyl]-3-oxo-2,5,8,11-tetraazatridecan-13-oato(3-)-N^5,N^8,N^{11},O^3,O^5,O^8, O^{11},O^{13}]gadolinium hydrate; trade name Omniscan, GE Healthcare) into the NMR sample to arrive at final concentrations of 0.25, 0.5, 1.0, 2.0, and 5.0 mM. A reference spectrum was recorded prior to the addition of spin label reagent.

Structure Calculation—Cross-peak intensities from NOESY experiments were translated into a continuous distribution of proton-proton distances. Based on the assigned tBid backbone chemical shifts, the TALOS program (52) was used to predict ϕ and ψ dihedral angles. The statistically significant dihedral angles in regular α-helical secondary structure were used as structural restraints. Generic hydrogen bond distance restraints were imposed for residues located at well defined α-helical regions. Additionally, PRE relaxation rates were calibrated over residue pairs within one single helix and converted into distances for structure calculation. The backbone T_1/T_2 relaxation ratios were also implemented into the structure calculation as previously described (53). Planar energy restraints for tBid residues with strong micelle interactions were also applied by mimicking a close distance with the membrane interface (54). tBid structures were calculated using simulated annealing protocol by the program Xplor-NIH (55). The final structure calculations employed 749 inter-residual and 180 intra-residual interproton distance restraints, 80 hydrogen bond distance restraints, 137 PRE distance restraints, 72 ϕ and 72 ψ angle restraints, 59 T_1/T_2 ratio restraints, and 28 planar energy restraints (Table 1). Structure presentation was prepared using PyMOL (56).

RESULTS

Secondary Structure of tBid in LPPG Micelles—tBid was produced by incubating purified modified full-length Bid with TEV protease instead of caspase-8 (25) (see "Experimental Procedures"). The choice of LPPG micelles to solubilize tBid for NMR characterization was made based on previous studies (37, 57) and a screen through various detergent micelles. The acquired two-dimensional ^{1}H,^{15}N-HSQC spectrum of tBid in NMR buffer with 8% LPPG at 45 °C showed varying peak intensities suggesting tBid residues might experience different effective rotational correlation times. This is likely due to their different states of association with the micelles. Analysis of the NMR datasets yielded near complete backbone and side chain resonance assignments of tBid. As many as 125 of 131 non-proline tBid backbone amides were assigned and only residues at the N terminus (Asn^{62} to His^{66}) were not assigned due to the exchange with the solvent. The $^1H^N$ NMR resonances of tBid showed a small dispersion, indicating the presence of mostly

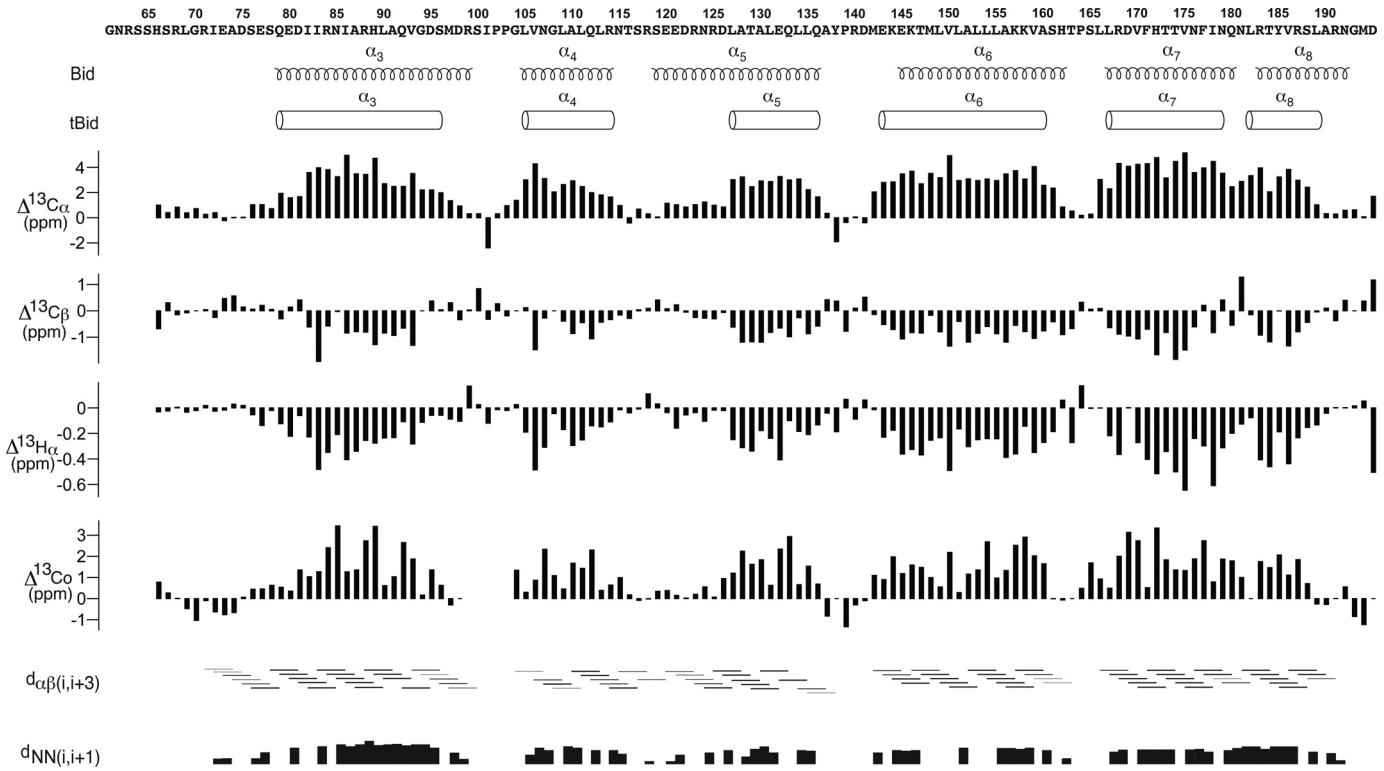

FIGURE 1. **Secondary structures of human tBid in LPPG micelles.** The secondary chemical shift index ($^{13}C\alpha$, $^{13}C\beta$, $^{1}H\alpha$, and ^{13}CO) defined the presence of six α-helices. The chemical shift differences were calculated by subtracting the average random coil chemical shift from the assigned tBid chemical shift values. The consecutive large positive bars in $^{13}C\alpha$,^{13}CO and negative bars in $^{13}C\beta$,$^{1}H\alpha$ suggest the presence of the α-helical conformation. The defined α-helices were also indicated by the characteristic medium range inter-proton NOE connectivities of $H\alpha^{i}$ to $H\beta^{i+3}$ and strong NOE connectivities of H_N^{i} to H_N^{i+1}. The *thickness of bars* used to show NOE connectivities corresponds to the relative NOE intensity. The missing NOEs within the α-helical regions are due to overlapped peaks. The secondary structures of human Bid reported previously were also shown for comparison (32). Residue numbering is kept the same as the full-length Bid.

helical and random coil conformation. To be noted, the tBid C-terminal region (Ser^{188}–Asp^{195}) branched with another set of distinct resonance peaks with slightly weaker intensities, suggesting the flexible C-terminal tail experienced at least two distinct conformations.

The assigned Cα, Cβ, Hα, and CO secondary chemical shifts indicated the presence of six α-helices (α_3, 79–95; α_4, 105–114; α_5, 127–136; α_6, 143–160; α_7, 167–179; α_8, 182–189) (Fig. 1), which are further corroborated by the inter-proton NOE connectivity data. The overall secondary structural composition is similar to the previously reported NMR structure of cytosolic full-length human Bid (Fig. 1), but there are some obvious differences in the helical boundaries between tBid and Bid. The most significant difference comes from helix α_5. Compared with Bid, tBid helix α_5 is a shorter helix and residues Ser^{119}–Asp^{126} are in a loop conformation instead of α-helical conformation. Of note, weak helical inter-proton NOE distance ($H\alpha^{(i)}$ to $H\beta^{(i+3)}$) were observed for these residues (Ser^{119}–Asp^{126}), suggesting a residual α-helical character (Fig. 1). This particular feature was also observed for tBid residues adjacent to the N-terminal end of helix α_3.

Backbone Dynamics of tBid in LPPG Micelles—The backbone ^{15}N T_1 and T_2 relaxations were measured for tBid at both 800 and 600 MHz proton resonance frequencies. The backbone ^{15}N T_2 relaxation data indicated that all tBid helical regions are rigid compared with the non-helical regions (Fig. 2*B*), and show similar diffusive behavior. This implies that these rigid helices tumble together with the micelle. In contrast, the loop between helices α_4 and α_5 (Asn^{115}–Asp^{126}) are highly flexible with high T_2 and low T_1 values (Fig. 2), similar to flexible N and C termini. The average T_1 and T_2 relaxation times for the rigid helical regions at 800 MHz frequency are 1.55 ± 0.21 s and 38.2 ± 4.1 ms, respectively. The calculated T_1/T_2 ratios (data not shown) gave an estimate of rotational correlation time (τ_c) of 16.0 ns, which is roughly equivalent to a globular protein with a molecular mass of 43 kDa in solution. The variations in T_1/T_2 ratios (data not shown) for the helices in tBid indicate that the molecule is quite anisotropic in LPPG micelles. It is also worth noting that tBid helices α_6 and α_7 have shorter ^{15}N T_2 values (33.3 ± 1.1 ms) and higher T_1/T_2 ratios (55.0 ± 2.9) at 800 MHz frequency than the rest of the helices observed (Fig. 2). The similar T_1/T_2 ratios also suggested helices α_6 and α_7 have comparable effective correlation times and orient similarly to each other with respect to the rotational diffusion axis. To identify residues that experience large amplitude fast motion, residue specific order parameters (S^2) were calculated by fitting the relaxation data obtained at the two magnetic fields (Fig. 2*C*). As expected the exposed loops between helices α_3-α_4, α_4-α_5, and α_5-α_6 have low S^2, in addition to the termini. All helices show no evidence of large amplitude fast motion. The initial probe for possible conformational exchange was done by evaluating the ratio of T_2 values obtained at 600 *versus* 800 MHz (data not shown). Residues whose T_2 ratio lies outside the 1.5 times S.D. from the average value are Asn^{85}, Ile^{86}, Leu^{149}, Ala^{156}, Gly^{193}, Met^{194}, and Asp^{195}. Residues Asn^{85} and Ile^{86} are in helix α_3, however, their T_2 ratios are not significantly outside the cutoff.

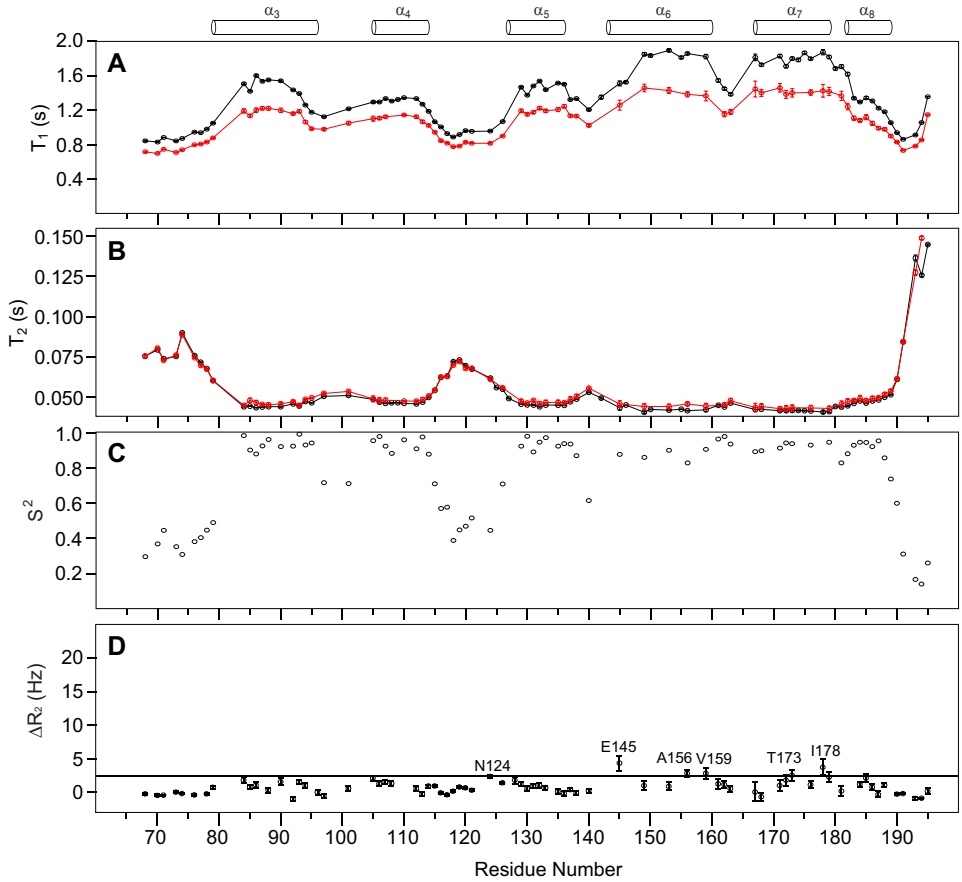

FIGURE 2. **Backbone ^{15}N relaxation dynamics of human tBid in LPPG micelles.** tBid ^{15}N T_1 (*A*) and T_2 (*B*) relaxation times at two magnetic fields of 600 MHz (*red*) and 800 MHz (*black*) and the fitted backbone order parameter S^2 using measured T_1 and T_2 data at both magnetic fields (*C*) are plotted as a function of residue number, indicating all six (α_{3-8}) helical regions were shown to be rigid. The shorter T_2 values (*B*) for both helices α_6 and α_7 suggested they are likely more embedded in the micelle. *Error bar* for the ^{15}N T_1 and T_2 relaxation data were estimated as previously described (50). *D*, the residues undergoing microsecond-millisecond conformational exchange identified using the backbone ^{15}N R_2-CPMG rate differences, ΔR_2, the difference between measurements at two different τ_{cp} values ($\Delta R_2 = R_2$ (6 ms) $- R_2$ (0.3 ms)). The cutoff line corresponds to the ΔR_2 threshold of 1.5 times the S.D. The missing values are due to resonance peak overlap. Secondary structure elements of tBid are indicated at the *top* for reference.

Although residues Leu^{149} and Ala^{156} are in α_6, and Gly^{193}, Met^{194}, and Asp^{195} are at the C-terminal all show significant deviation. To identify additional residues that might be undergoing conformational exchange as well as to confirm those identified by the T_2 ratio at the two magnetic fields, relaxation dispersion experiments were carried out. The relaxation dispersion data (Fig. 2*D*) suggested a few residues (Asn^{124}, Glu^{145}, Ala^{156}, Val^{159}, Thr^{173}, and Ile^{178}) undergo microsecond-millisecond time scale exchange. They are identified by choosing a cutoff of ΔR_2 beyond the 1.5 times S.D. Residues Glu^{145}, Ala^{156}, and Val^{159} suggest tBid helix α_6 is likely to experience some conformational exchange, which is consistent with the T_2 ratio data. Of note, residue Asn^{124} at the loop between helices α_4-α_5 and Thr^{173} and Ile^{178} at helix α_7 are also shown to undergo conformational exchange.

tBid Adopts a C-shape Conformation in LPPG Micelles—The near complete assignments of the inter-proton cross-peak NOE dataset yielded 931 NOEs. Analysis of these inter-proton NOEs did not produce any long-range contacts (greater than 5 residues apart). The absence of long-range NOEs renders the determination of tertiary fold of the six α-helices tBid structure impossible. Therefore, longer distance oriented PRE experiments were performed. Paramagnetic spin labels were incorporated at three tBid sites with cysteine mutations (S78C, Q136C, and Q180C). The backbone ^1H_N-Γ_2 rate measurements were carried out and the results showed residues close to the paramagnetic center experienced obvious enhancement (Fig. 3). For the S78C sample, weak enhancements were shown for residues at the tBid C terminus, suggesting a close conformation but with no NOE contact (<5 Å) between the tBid N and C terminus (Fig. 3). Consistently, weaker PRE effects were shown for tBid N-terminal residues to the C-terminal spin label at residue 180 (Q180C sample). For Q136C, weak PRE effects were observed for residues in helices α_4 and α_5 as well as some residues in the N and C termini (Fig. 3). Another possible contribution to the observed PRE effects is due to intermolecular contacts. To address whether tBid homo-oligomerizes in LPPG micelles, PRE measurements by mixing ^{15}N-labeled wild type tBid with spin-labeled ^{14}N-tBid at equal molar ratios were carried out and no obvious enhancement was observed for both S78C and Q136C samples (data not shown). This implied no inter-molecular contact between tBid monomers and therefore tBid does not homo-oligomerize and is monomeric in LPPG micelles.

All tBid Helices Are Involved in the Interaction with LPPG Micelles—To understand the molecular interaction between tBid and LPPG micelles, a perdeuterated ^{15}N-labeled tBid was

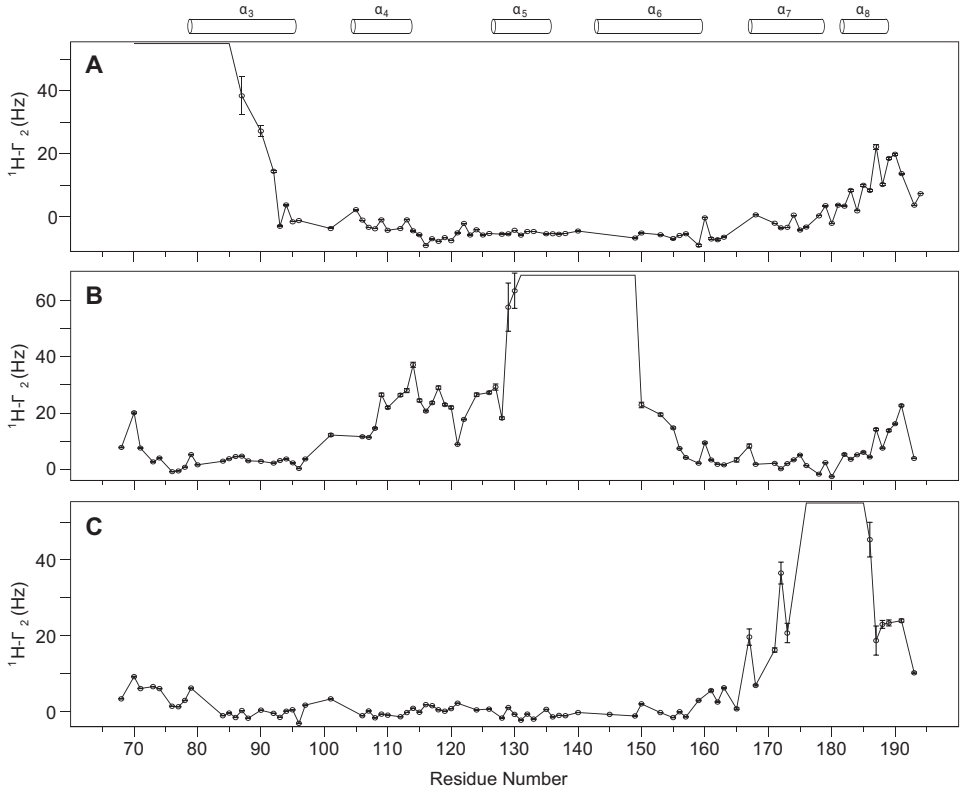

FIGURE 3. **Measured PRE effects for human tBid cysteine mutants in LPPG micelles at three different sites.** The experimental ^1H_N-Γ_2 values for S78C (*A*), Q136C (*B*), and Q180C (*C*) were plotted as the function of residue number. Residues experiencing significant PRE effects are mainly localized to residues that are close to the paramagnetic center. For the S78C sample (*A*), weak PRE effects for residues in the C terminus included helix α_8. *C,* albeit even weaker, similar weak PRE effects were also observed between the tBid N terminus and C terminus. For the Q136C sample (*B*), weak PRE effects were observed for residues in helices α_4 and α_4 as well as some residues in flexible N and C termini. *Error bars* were estimated as previously described (51). Secondary structure elements of tBid are indicated at the *top* for reference.

prepared in LPPG micelles. The three-dimensional ^{15}N-edited NOESY-HSQC experiment was carried out to detect direct NOE interactions between the protein backbone amide protons and protons from LPPG micelles. The LPPG molecule possesses a long acyl chain with abundant methylene protons, which gives a dominant ^{1}H NMR signal at a chemical shift of 1.26 ppm (Fig. 4*A*). Extensive analysis of the NOE cross-peaks at this chemical shift yielded a residue-specific protein-micelle interaction profile. Due to overlaps with the signals from some tBid Thr Hγ_2 or Ile Hγ_1 protons because of incomplete deuteration, we simply omitted those residues for further consideration of possible protein-micelle interactions. In the end, 28 tBid residues with obvious protein-micelle interactions were identified (Fig. 4*B*). These tBid residues are mostly hydrophobic residues and are scattered over all six tBid helices: α_3 (Ile^{86}, Ala^{87}, Leu^{90}, Val^{93}, and Gly^{94}), α_4 (Val^{106}, Leu^{109}, Ala^{110}, Leu^{113}), α_5 (Leu^{127}, Leu^{131}, Leu^{135}), Tyr^{138}, α_6 (Leu^{149}, Leu^{153}, Ala^{156}, Lys^{157}, Val^{159}, Ala^{160}), Ser^{161}, α_7 (Leu^{167}, Arg^{168}, Phe^{171}, His^{172}, Val^{175}, Asn^{179}), and α_8 (Leu^{182}, Val^{186}). This strongly suggested those rigid tBid helices are embedded in LPPG micelles through extensive hydrophobic interactions. Among those identified, residues in helix α_6 and α_7 showed noticeably higher relative NOE intensities, suggesting both helices are more embedded in LPPG micelles than other tBid helices (Fig. 4*B*). This is consistent with previous EPR studies that showed tBid helices α_{6-8} are membrane-associated (34). Of note, three positively charged residues (Lys^{157}, Arg^{168}, and His^{172}) in these two helices also showed strong micelle interactions. Surprisingly, the BH_3 domain containing helix α_3, which was previously proposed to be exposed and outside the membrane surface, also show extensive micelle interactions (Fig. 4*A*). Taken together, tBid helices α_{3-5} and α_8 showed a consistent micelle interaction pattern for hydrophobic residues located at one side of the helix, suggesting tBid helices are embedded parallel to the membrane surface. In contrast, residues (Ser^{76}, Glu^{77}, Ser^{78}, Gln^{79}, Arg^{118}, Ser^{119}, Glu^{120}, Glu^{121}, Asn^{124}, and Gly^{193}) in tBid flexible regions including the long loop (Asn^{115}–Asp^{126}) between helix α_4 and α_5 clearly did not show any obvious interaction with the micelles. This observation was further corroborated with the strong protein-water interaction for this flexible region (data not shown). In addition, the solvent PRE experiments were carried out and showed consistent limited water accessibility, which is a weak solvent PRE effect, for residues that are lipid embedded for all tBid helices and a strong PRE effect for water-exposed residues (Fig. 4*C*).

Structure of tBid in LPPG Micelles—Structure calculation of tBid were carried out using the following NMR restraints: NOE-derived distances, TALOS-derived dihedral angles, generic hydrogen bonds, PRE-derived distances, and T_1/T_2 derived relaxation restraints (Table 1). With the assumption that tBid helices are embedded parallel to the membrane surface, tBid residues that showed a strong micelle interaction were also implemented into the structure calculation with residue-specific planar energy restraints. The calculated 20 lowest

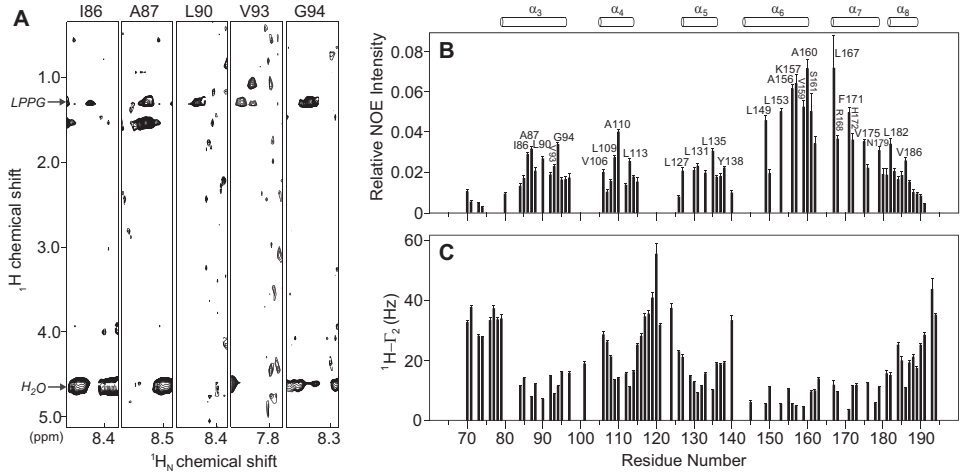

FIGURE 4. **Interactions between human tBid and LPPG micelles.** *A*, illustration of inter-proton NOEs between the tBid BH_3 domain and LPPG micelles. A selection of the ^{15}N-edited three-dimensional NOESY-HSQC strips of the tBid BH_3 domain, containing helix α_3 residues, showing the intermolecular NOEs to the LPPG acyl chain ^1H at a chemical shift of 1.26 ppm. Among these residues, Ile^{86}, Ala^{87}, Leu^{90}, Val^{93}, and Gly^{94} showed obvious NOE cross-peaks to LPPG micelles. Conversely, these residues did not show an obvious cross-peaks signal to water (4.61 ppm). *B*, relative peak intensities are calculated by taking the ratios of measured NOE intensities between protein backbone amides (^1H_N) and the LPPG acyl chain methylene (CH_2) groups at 1.26 ppm against the diagonal peak intensities. These relative peak intensity ratios are used to quantify the strength of interaction between various sites in tBid and micelles. Residues showing obvious protein-lipid interactions are from all six tBid helices (α_{3-8}). *C*, the experimental solvent PRE measurement for tBid backbone amide protons. The measured ^1H_N-Γ_2 PRE values in the presence of a water-soluble paramagnetic probe showed obvious relaxation enhancement for residues that are water exposed and weak enhancement for residues that are embedded in the lipid. Secondary structure elements of tBid are indicated at the *top* for reference.

TABLE 1

Structural statistics of the human tBid in LPPG micelles

Statistics are given for the 20 lowest energy structures out of 200 calculated NMR structures.

Distance restraints (Å)	
NOE (930)[a]	0.021 ± 0.003
Intraresidual NOE (180)	0.007 ± 0.007
Sequential NOE ($\|i-j\| = 1$) (298)	0.018 ± 0.003
Medium range ($2 \leq \|i-j\| \leq 5$) (451)	0.025 ± 0.006
H-bonds (80)	0.028 ± 0.004
Paramagnetic relaxation enhancement (137)	0.017 ± 0.006
Dihedral angle restraints (°)	0.207 ± 0.050
ϕ (72)	0.157 ± 0.054
ψ (72)	0.241 ± 0.070
Other restraints	
Plane energy (Å) (28)	0.75 ± 0.17
T_1/T_2 ratio (59)	25.48 ± 3.62
Coordinate precision r.m.s. deviation[b]	
Backbone (Å)	3.64 ± 1.37
Heavy atoms (Å)	4.24 ± 1.36
Ramachandran plot	
Most favored regions	79.0 ± 2.3%
Allowed regions	14.1 ± 2.4%
Generously allowed regions	4.0 ± 2.0%
Disallowed regions	2.9 ± 1.5%

[a] Number in parentheses corresponds to the total number of restraints.
[b] The r.m.s. deviation values were calculated by superimposing all six α-helices.

energy tBid structures show well defined individual helices (α_3 to α_8) with backbone r.m.s. deviations of 0.45 ± 0.16, 0.47 ± 0.13, 0.29 ± 0.09, 0.38 ± 0.15, 0.32 ± 0.10, and 0.41 ± 0.11 Å, respectively. As previously noted the absence of long-range NOE restraints left the tBid global conformation to be mainly defined by long-range PRE restraints. This resulted in calculated tBid structures with a backbone r.m.s. deviation of 3.64 ± 1.37 Å when superimposing all six tBid helices (Fig. 5*A*). The calculated tBid structures adopted an extended conformation with the N-terminal end being close but without direct atomic contact to the C terminus, thus forming a C-shape structure (Fig. 5, *A* and *B*). Relative to the membrane interface, tBid helices formed two faces that showed dramatic differences in electrostatic surface potentials (Fig. 5*C*). One side of the tBid structure that faces the membrane shows dominant hydrophobic patches, which correspond to hydrophobic tBid residues that showed strong interactions to the LPPG micelles (Fig. 5*D*). Distinct electrostatic surfaces were shown on the other side of the tBid structure with many charged surfaces including BH_3 domain helix α_3 (Fig. 5*E*). With micelle-interacting residues (Ile^{86}, Ala^{87}, Leu^{90}, Val^{93}, and Gly^{94}) in helix α_3 facing toward the membrane surface, charged or polar residues (Asp^{81}, Arg^{84}, Arg^{88}, Gln^{92}, and Asp^{95}) are left facing away from the membrane surface for potential electrostatic interaction with other proteins (Fig. 5, *B* and *C*). Of note, strong positively charged surface areas were formed along tBid helices α_6-α_8 (Fig. 5*E*), which could potentially form electrostatic interactions with the negatively charged LPPG micelle head groups. This electrostatic interaction would prevent these helices to be completely buried inside the micelles. This is consistent with a previously suggested tBid conformation on the membrane by solid-state NMR studies (37). Overall, these structural features displayed by tBid in LPPG micelles are consistent with the fact that most tBid helices are amphipathic.

DISCUSSION

The cleavage of full-length Bid by caspase-8 forms the activated tBid, which can be translocated to the mitochondrial outer membrane (21). The association of tBid to membrane is critical for the promotion of apoptosis (18). Upon interaction with the hydrophobic environment *in vitro*, tBid undergoes conformational changes for favorable lipid interactions (34). Similar to full-length Bid, tBid was shown to be highly helical in various membrane mimics (37, 58, 59). Previously, membrane-associated tBid was shown to be parallel to the membrane surface with no transmembrane helix and the region bound to the membrane was suggested to be located at helices α_6-α_8 (34, 37). Those studies did not provide details on tBid helical boundaries

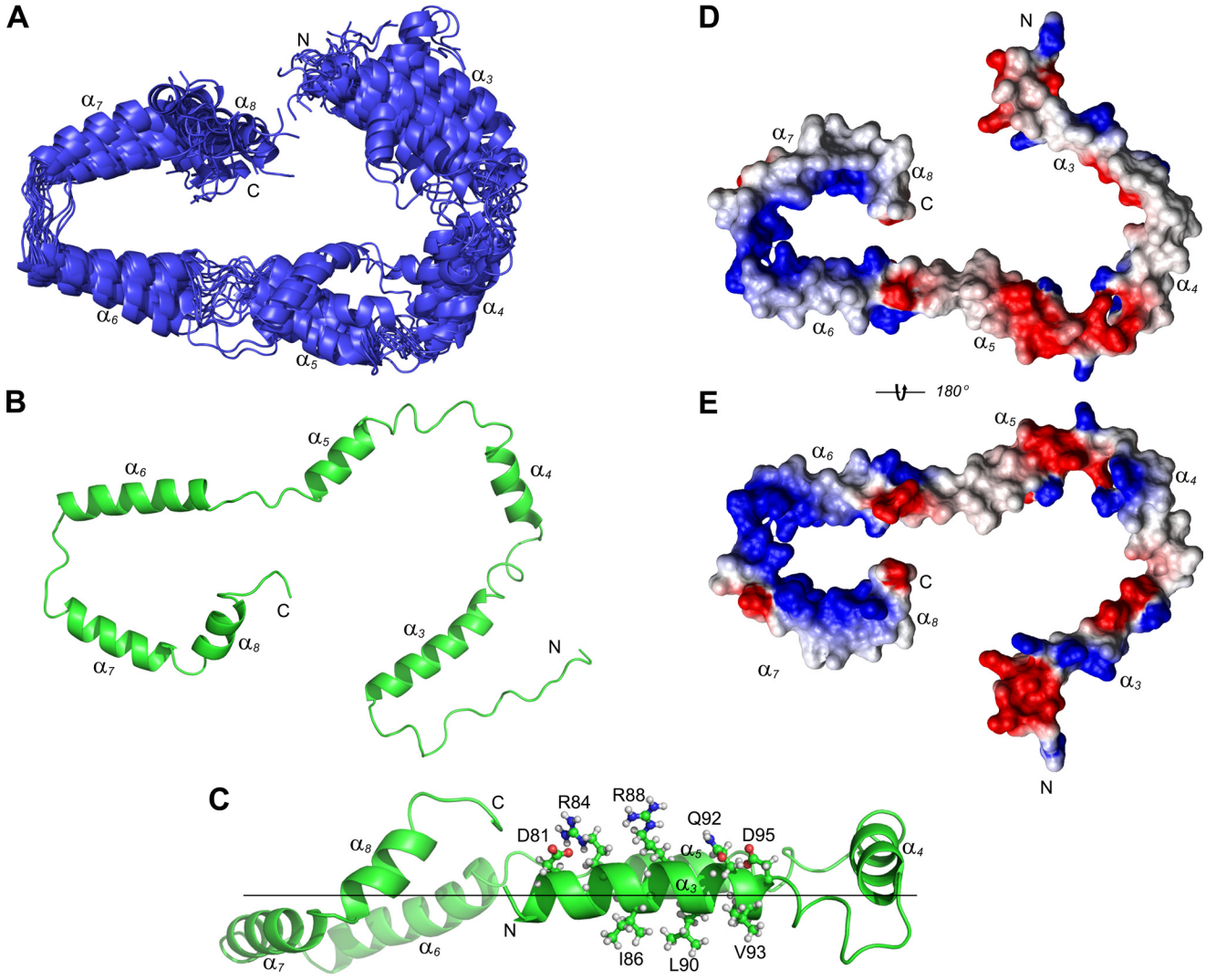

FIGURE 5. **Calculated human tBid structure shows a C-shape conformation.** *A,* schematic representation of the 20 lowest energy structures of human tBid in LPPG micelles. The calculated tBid structures show six well defined helices α_{3-8} and the superposition to the mean structure on tBid helical regions results in a backbone r.m.s. deviation of 3.64 Å. Both N-terminal (Gly^{61}–Ser^{78}) and C-terminal (Ala^{190}–Asp^{195}) tails are unstructured and are omitted for clarity. Overall (*B*) tBid adopts a C-shape structure with both N and C termini in close conformation. *C,* tBid helices (α_{3-8}) are parallel to the putative membrane surface with helices α_6 and α_7 more embedded. For the membrane-associated tBid helix α_3, charged or polar residues (Asp^{81}, Arg^{84}, Arg^{88}, Gln^{92}, and Asp^{95}) are facing away from the membrane surface and are exposed for potential interactions with other proteins. *C,* on the opposite side of helix α_3 residues (Ile^{86}, Ala^{87}, Leu^{90}, Val^{93}, and Gly^{94}) with strong micelle interactions are facing toward the membrane surface. The flexible N terminus (Gly^{61}–Ser^{78}) was omitted for clarity. *D,* electrostatic potential surface view of the side of the tBid structure facing the membrane shows dominant hydrophobic patches along the ordered tBid helices. *E,* the opposite side of the tBid surface shows strong charged areas along tBid helices with a continuous positive charged surface along the helices α_6-α_8. *D* and *E,* the flexible loop with a highly charged surface between helix α_4 and helix α_5 contains a number of charged residues.

and the membrane-associated full-length tBid structure at the atomic level. Especially, no structural information on the functionally important BH_3 domain is yet available. This renders understanding of the precise apoptotic function of tBid and its molecular interactions with Bax/Bak or Bcl-xL on the membrane impossible. To fill this gap, we determined the solution structure of full-length human tBid in a lipid membrane mimic, LPPG micelles by NMR.

Secondary structure characterization by NMR demonstrated that tBid has six well defined helices, which are mostly preserved from the full-length Bid (Fig. 1). However, some obvious differences were observed between full-length Bid and tBid in LPPG micelles. For instance, tBid residues (Ser^{119}–Asp^{126}) close to the N-terminal end of helix α_5 did not form a rigid helix (Fig. 1). Compared to the full-length Bid structure, the loop between helices α_4 and α_5 is much shorter (32) than the loop in tBid. This extended tBid loop between helices α_4 and α_5 was shown to be highly flexible and did not show any interaction with the micelles, contrasting to the rigid helical conformation in Bid (Figs. 1 and 4). The highly flexible behavior of this loop is likely due to the presence of many charged residues (Arg^{118}, Glu^{120}, Glu^{121}, Asp^{122}, Arg^{123}, Arg^{125}, and Asp^{126}), which could potentiate electrostatic interactions of tBid with other protein(s). Recent peptide screening proposed an important role for this flexible tBid region (60), through which tBid can directly interact with the protein MTCH2 (mitochondrial carrier homologue 2) (36, 61). The exposure of this flexible tBid loop enables a scenario where the interaction between tBid and MTCH2 is likely to occur at the mitochondria outer membrane.

The analysis of tBid NOE data did not produce any long-range NOEs, indicating that six well defined tBid helices do not form a compact structure (Fig. 5). Long distance-oriented PRE measurements, however, showed some distances between the tBid N and C termini within 20–25 Å (Fig. 3). These distances impose a C-shape conformation for tBid on LPPG micelles surface. A rather similar result was also seen previously for the micelle-bound α-synuclein (62) with a contrast that tBid is more complex with 6 helices. The size of the LPPG micelle was estimated to have a diameter of ~68 Å (63). At the longest circumference, it is considerably too large for tBid to wrap around it and form a C-shape configuration as described (Fig. 5). Based on our experimental data, however, we believe the C-shape conformation of tBid is likely due to its characteristic interaction with the curved LPPG micelle membrane within one constrained area on the micelle hemisphere. This is consistent with previous findings that tBid could colocalize with cardiolipin, a mitochondrial lipid that was previously suggested to induce mitochondrial membrane curvatures (5), at the mitochondrial outer membrane contact sites with "curvature stress" (64). Therefore, tBid could be attracted to the contact sites with membrane curvatures on the mitochondria outer membrane, hence sensitizing the mitochondrial membrane for Bax-induced membrane permeabilization.

The tBid α_6 helix contains a stretch of hydrophobic residues (^{148}MLVLALLLA^{156}) and were predicted to be membrane-associated. Our data indeed showed strong micelle interactions for hydrophobic residues in tBid helix α_6 and α_7 as well (Fig. 4). The actual tBid membrane interaction site was suggested to be at the mitochondrial contact site with clustered negatively charged lipid cardiolipin (64–72). The negatively charged LPPG was chosen not only to provide the best working sample, but as a relevant mimic to the cardiolipin-rich mitochondrial membrane as well. Positively charged lysine residues (Lys^{157} and Lys^{158}) in tBid helix α_6 were suggested to be critical for a specific electrostatic interaction with the mitochondrial outer membrane (71, 72). Our data confirmed this hypothesis by showing a strong micelle interaction for tBid residue lysine 157 as well as charged residues Arg^{168} and His^{172} in helix α_7 (Fig. 4). Consistently, the electrostatic surface map of the tBid structure further showed continuous positively charged surfaces along helices α_{6-8} (Fig. 5), which might form electrostatic interactions with negatively charged lipid cardiolipin headgroups on the membrane. Furthermore, this additional electrostatic interaction may account for our findings that both helix α_6 and α_7 are more membrane embedded than the rest of tBid helices (Figs. 2 and 4) and implicate a membrane recognition and docking role for these two helices. The recently reported fluorescence data showed tBid regions corresponding to Bid helix α_{4-7} are membrane embedded and also suggested a conformational equilibrium between two major states of tBid (36). Our structure, which show all tBid helices are membrane associated, is consistent with their findings. Furthermore, to be in equilibrium of multiple conformations, the tBid structure must have a considerable degree of flexibility. Our structure and dynamic data support this possibility. We showed that tBid adopted an extended membrane-associated structure that contains flexible loops connecting helices α_3-α_4, α_4-α_5, and α_5-α_6. In addition, we also showed that some residues in helix α_6 (Leu^{149}, Ala^{156}, and Val^{159}) and at its N-terminal (Glu^{145}), the site of membrane targeting, undergo conformational exchange. This result seems to be supporting the conformational equilibrium observation by the fluorescence measurement.

A previous model proposed that the tBid BH_3 domain was fully exposed and located above the membrane surface, poised for protein interactions with Bax/Bak or Bcl-xL (35). However, our studies revealed that the important BH_3 domain containing helix α_3 was membrane associated with hydrophobic residues facing toward the membrane surface (Figs. 4 and 5*E*). In contrast to the latest suggested solvent-exposed BH_3 domain (36), our data presented an energetically more favorable conformation for the tBid BH_3 domain that is membrane-associated due to its residue composition. Therefore, our structure supports a scenario that the interaction between the membrane-associated helical BH_3 domain and Bax happens on the membrane surface. The on the membrane interaction is consistent with previous observations that membrane-targeted tBid BH_3 peptides can still effectively interact with and activate Bax to permeabilize mitochondrial membranes (38, 73). Previous studies also suggested that Bax helix α_1 interacts with the tBid BH_3 domain as the first step in its tBid-induced activation (28, 74). Upon contact with the membrane surface, Bax was suggested to experience a reversible conformational change and its N terminus can get exposed and recognized by the conformation-specific antibody 6A7 (75). The subsequent membrane insertion and activation of Bax was shown to involve the interaction with membrane-associated tBid (18). It is possible that the tBid BH_3 domain interacts with the transiently exposed Bax helix α_1 on the membrane surface and this specific interaction can shift the reversible conformational change of membrane-encountered Bax into a membrane-associated state. In fact, a specific electrostatic interaction between tBid BH_3 domain residue Arg^{84} and Bax helix α_1 residue Asp^{33} was reported to be important for tBid-induced Bax activation in a previous study (74). Therefore, our results of the tBid structure in LPPG micelles in combination with the above reported findings lead to the possibility that charged residues in the tBid BH_3 domain (Asp^{81}, Arg^{84}, Arg^{88}, and Asp^{95}) that were shown to face away from the membrane could potentially form electrostatic interactions with charged residues (Asp^{33} and Arg^{34}) in Bax helix α_1 on the membrane surface. If the conventional BH_3 binding mode to Bax is required (19, 76–78), then the interaction has to occur in such a way to allow the hydrophobic tBid BH_3 residues to be available to bind Bax. One possible scenario would be that the electrostatic interactions between the tBid BH_3 domain and Bax helix α_1 could promote displacement of the tBid BH_3 residues from the lipid membrane, exposing them for binding to the Bax BH_3 binding pocket.

For Bcl-xL, it is difficult to discuss its interaction with tBid on the membrane with very limited information on membrane-associated Bcl-xL. However, it is likely that a similar interaction between tBid and Bcl-xL on the mitochondrial membrane was adopted as in the tBid-Bax interaction given the structural similarity between Bax and Bcl-xL.

Overall, Our data provided novel molecular information regarding the structure and dynamics of tBid in LPPG micelles,

which leads to a first step in understanding the tBid apoptotic function on the mitochondrial membrane. Although our findings did not directly address the favorability of a direct or indirect activation model, the membrane-embedded tBid BH_3 domain suggested an on the membrane binding mode of tBid with Bax, thus leaning toward the previously proposed embedded together model (13). The recently solved x-ray structure of the Bax dimer promoted by the tBid BH_3 peptide and detergent provided valuable information on the tBid-induced Bax activation (79). The reported binding mode with the tBid BH_3 peptide sitting inside the hydrophobic BH_3-binding cleft of Bax is essentially similar to inter-protein interactions among Bcl-2 family members in solution (19, 76, 77). Nevertheless, how the tBid BH_3 domain, shown in our study to be associated with the micelles, can go into the BH_3 binding pocket of Bax still remains unclear. Further elucidation of the tBid-Bax complex structure on the membrane will provide more molecular details on the mechanism of tBid-mediated Bax activation.

Acknowledgments—We are very grateful to Dr. Motoshi Suzuki for technical help and valuable discussion on the project and Dr. Charles D. Schwieters for help on restraint implementation in Xplor-NIH. We also thank Dr. Duck-Yeon Lee (Biochemistry Core Facility, NHLBI, National Institutes of Health) for expertise and advice regarding the mass spectrometry-related experiments performed in this paper. We thank Dr. Francesca Marassi for providing the Bid cDNA.

REFERENCES

1. Danial, N. N., and Korsmeyer, S. J. (2004) Cell death. Critical control points. *Cell* **116,** 205–219
2. Wang, X. (2001) The expanding role of mitochondria in apoptosis. *Genes Dev.* **15,** 2922–2933
3. Youle, R. J., and Strasser, A. (2008) The BCL-2 protein family. Opposing activities that mediate cell death. *Nat. Rev. Mol. Cell Biol.* **9,** 47–59
4. Adams, J. M. (2003) Ways of dying. Multiple pathways to apoptosis. *Genes Dev.* **17,** 2481–2495
5. Kuwana, T., Mackey, M. R., Perkins, G., Ellisman, M. H., Latterich, M., Schneiter, R., Green, D. R., and Newmeyer, D. D. (2002) Bid, Bax, and lipids cooperate to form supramolecular openings in the outer mitochondrial membrane. *Cell* **111,** 331–342
6. Wei, M. C., Zong, W. X., Cheng, E. H., Lindsten, T., Panoutsakopoulou, V., Ross, A. J., Roth, K. A., MacGregor, G. R., Thompson, C. B., and Korsmeyer, S. J. (2001) Proapoptotic BAX and BAK. A requisite gateway to mitochondrial dysfunction and death. *Science* **292,** 727–730
7. Marani, M., Tenev, T., Hancock, D., Downward, J., and Lemoine, N. R. (2002) Identification of novel isoforms of the BH3 domain protein Bim which directly activate Bax to trigger apoptosis. *Mol. Cell Biol.* **22,** 3577–3589
8. Sattler, M., Liang, H., Nettesheim, D., Meadows, R. P., Harlan, J. E., Eberstadt, M., Yoon, H. S., Shuker, S. B., Chang, B. S., Minn, A. J., Thompson, C. B., and Fesik, S. W. (1997) Structure of Bcl-xL-Bak peptide complex. Recognition between regulators of apoptosis. *Science* **275,** 983–986
9. García-Sáez, A. J., Ries, J., Orzáez, M., Pérez-Payà, E., and Schwille, P. (2009) Membrane promotes tBID interaction with BCL-X_L. *Nat. Struct. Mol. Biol.* **16,** 1178–1185
10. Kuwana, T., Bouchier-Hayes, L., Chipuk, J. E., Bonzon, C., Sullivan, B. A., Green, D. R., and Newmeyer, D. D. (2005) BH3 domains of BH3-only proteins differentially regulate Bax-mediated mitochondrial membrane permeabilization both directly and indirectly. *Mol. Cell* **17,** 525–535
11. Willis, S. N., Fletcher, J. I., Kaufmann, T., van Delft, M. F., Chen, L., Czabotar, P. E., Ierino, H., Lee, E. F., Fairlie, W. D., Bouillet, P., Strasser, A., Kluck, R. M., Adams, J. M., and Huang, D. C. (2007) Apoptosis initiated when BH3 ligands engage multiple Bcl-2 homologs, not Bax or Bak. *Science* **315,** 856–859
12. Llambi, F., Moldoveanu, T., Tait, S. W., Bouchier-Hayes, L., Temirov, J., McCormick, L. L., Dillon, C. P., and Green, D. R. (2011) A unified model of mammalian BCL-2 protein family interactions at the mitochondria. *Mol. Cell* **44,** 517–531
13. Leber, B., Lin, J., and Andrews, D. W. (2007) Embedded together. The life and death consequences of interaction of the Bcl-2 family with membranes. *Apoptosis* **12,** 897–911
14. Letai, A., Bassik, M. C., Walensky, L. D., Sorcinelli, M. D., Weiler, S., and Korsmeyer, S. J. (2002) Distinct BH3 domains either sensitize or activate mitochondrial apoptosis, serving as prototype cancer therapeutics. *Cancer Cell* **2,** 183–192
15. Kim, H., Rafiuddin-Shah, M., Tu, H. C., Jeffers, J. R., Zambetti, G. P., Hsieh, J. J., and Cheng, E. H. (2006) Hierarchical regulation of mitochondrion-dependent apoptosis by BCL-2 subfamilies. *Nat. Cell Biol.* **8,** 1348–1358
16. Hsu, Y. T., Wolter, K. G., and Youle, R. J. (1997) Cytosol-to-membrane redistribution of Bax and Bcl-X_L during apoptosis. *Proc. Natl. Acad. Sci. U.S.A.* **94,** 3668–3672
17. Bogner, C., Leber, B., and Andrews, D. W. (2010) Apoptosis. Embedded in membranes. *Curr. Opin. Cell Biol.* **22,** 845–851
18. Lovell, J. F., Billen, L. P., Bindner, S., Shamas-Din, A., Fradin, C., Leber, B., and Andrews, D. W. (2008) Membrane binding by tBid initiates an ordered series of events culminating in membrane permeabilization by Bax. *Cell* **135,** 1074–1084
19. Petros, A. M., Olejniczak, E. T., and Fesik, S. W. (2004) Structural biology of the Bcl-2 family of proteins. *Biochim. Biophys. Acta* **1644,** 83–94
20. Wang, K., Yin, X. M., Chao, D. T., Milliman, C. L., and Korsmeyer, S. J. (1996) BID. A novel BH_3 domain-only death agonist. *Genes Dev.* **10,** 2859–2869
21. Luo, X., Budihardjo, I., Zou, H., Slaughter, C., and Wang, X. (1998) Bid, a Bcl2 interacting protein, mediates cytochrome *c* release from mitochondria in response to activation of cell surface death receptors. *Cell* **94,** 481–490
22. Li, H., Zhu, H., Xu, C. J., and Yuan, J. (1998) Cleavage of BID by caspase 8 mediates the mitochondrial damage in the Fas pathway of apoptosis. *Cell* **94,** 491–501
23. Boldin, M. P., Goncharov, T. M., Goltsev, Y. V., and Wallach, D. (1996) Involvement of MACH, a novel MORT1/FADD-interacting protease, in Fas/APO-1- and TNF receptor-induced cell death. *Cell* **85,** 803–815
24. Muzio, M., Chinnaiyan, A. M., Kischkel, F. C., O'Rourke, K., Shevchenko, A., Ni, J., Scaffidi, C., Bretz, J. D., Zhang, M., Gentz, R., Mann, M., Krammer, P. H., Peter, M. E., and Dixit, V. M. (1996) FLICE, a novel FADD-homologous ICE/CED-3-like protease, is recruited to the CD95 (Fas/APO-1) death-inducing signaling complex. *Cell* **85,** 817–827
25. Zha, J., Weiler, S., Oh, K. J., Wei, M. C., and Korsmeyer, S. J. (2000) Post-translational *N*-myristoylation of BID as a molecular switch for targeting mitochondria and apoptosis. *Science* **290,** 1761–1765
26. Ott, M., Norberg, E., Zhivotovsky, B., and Orrenius, S. (2009) Mitochondrial targeting of tBid/Bax. A role for the TOM complex? *Cell Death Differ.* **16,** 1075–1082
27. Eskes, R., Desagher, S., Antonsson, B., and Martinou, J. C. (2000) Bid induces the oligomerization and insertion of Bax into the outer mitochondrial membrane. *Mol. Cell Biol.* **20,** 929–935
28. Kim, H., Tu, H. C., Ren, D., Takeuchi, O., Jeffers, J. R., Zambetti, G. P., Hsieh, J. J., and Cheng, E. H. (2009) Stepwise activation of BAX and BAK by tBID, BIM, and PUMA initiates mitochondrial apoptosis. *Mol. Cell* **36,** 487–499
29. Epand, R. F., Martinou, J. C., Fornallaz-Mulhauser, M., Hughes, D. W., and Epand, R. M. (2002) The apoptotic protein tBid promotes leakage by altering membrane curvature. *J. Biol. Chem.* **277,** 32632–32639
30. Schendel, S. L., Azimov, R., Pawlowski, K., Godzik, A., Kagan, B. L., and Reed, J. C. (1999) Ion channel activity of the BH3 only Bcl-2 family member, BID. *J. Biol. Chem.* **274,** 21932–21936
31. Grinberg, M., Sarig, R., Zaltsman, Y., Frumkin, D., Grammatikakis, N., Reuveny, E., and Gross, A. (2002) tBID homooligomerizes in the mitochondrial membrane to induce apoptosis. *J. Biol. Chem.* **277,** 12237–12245
32. Chou, J. J., Li, H., Salvesen, G. S., Yuan, J., and Wagner, G. (1999) Solution

structure of BID, an intracellular amplifier of apoptotic signaling. *Cell* **96,** 615–624
33. McDonnell, J. M., Fushman, D., Milliman, C. L., Korsmeyer, S. J., and Cowburn, D. (1999) Solution structure of the proapoptotic molecule BID. A structural basis for apoptotic agonists and antagonists. *Cell* **96,** 625–634
34. Oh, K. J., Barbuto, S., Meyer, N., Kim, R. S., Collier, R. J., and Korsmeyer, S. J. (2005) Conformational changes in BID, a pro-apoptotic BCL-2 family member, upon membrane binding. A site-directed spin labeling study. *J. Biol. Chem.* **280,** 753–767
35. Billen, L. P., Shamas-Din, A., and Andrews, D. W. (2008) Bid. A Bax-like BH3 protein. *Oncogene* **27,** S93–104
36. Shamas-Din, A., Bindner, S., Zhu, W., Zaltsman, Y., Campbell, C., Gross, A., Leber, B., Andrews, D. W., and Fradin, C. (2013) tBid undergoes multiple conformational changes at the membrane required for Bax activation. *J. Biol. Chem.* **288**, 22111–22127
37. Gong, X. M., Choi, J., Franzin, C. M., Zhai, D., Reed, J. C., and Marassi, F. M. (2004) Conformation of membrane-associated proapoptotic tBid. *J. Biol. Chem.* **279,** 28954–28960
38. Oh, K. J., Barbuto, S., Pitter, K., Morash, J., Walensky, L. D., and Korsmeyer, S. J. (2006) A membrane-targeted BID BCL-2 homology 3 peptide is sufficient for high potency activation of BAX *in vitro*. *J. Biol. Chem.* **281,** 36999–37008
39. Grzesiek, S., and Bax, A. (1992) Improved 3D triple-resonance NMR techniques applied to a 31-kDa protein. *J. Magn. Reson.* **96,** 432–440
40. Grzesiek, S., and Bax, A. (1992) Correlating backbone amide and side chain resonances in larger proteins by multiple relayed triple resonance NMR. *J. Am. Chem. Soc.* **114,** 6291–6293
41. Wittekind, M., and Mueller, L. (1993) HNCACB, a high-sensitivity 3D NMR experiment to correlate amide-proton and nitrogen resonances with the α- and β-carbon resonances in proteins. *J. Magn. Reson. Ser. B* **101,** 201–205
42. Bax, A., and Grzesiek, S. (1993) Methodological advances in protein NMR. *Acc. Chem. Res.* **26,** 131–138
43. Kay, L. E., Xu, G. Y., and Yamazaki, T. (1994) Enhanced-sensitivity triple-resonance spectroscopy with minimal H_2O saturation. *J. Magn. Reson. Ser. A* **109,** 129–133
44. Clore, G. M., Kay, L. E., Bax, A., and Gronenborn, A. M. (1991) Four-dimensional $^{13}C/^{13}C$-edited nuclear Overhauser enhancement spectroscopy of a protein in solution. Application to interleukin 1β. *Biochemistry* **30,** 12–18
45. Barbato, G., Ikura, M., Kay, L. E., Pastor, R. W., and Bax, A. (1992) Backbone dynamics of calmodulin studied by ^{15}N relaxation using inverse detected two-dimensional NMR spectroscopy. The central helix is flexible. *Biochemistry* **31,** 5269–5278
46. Iwahara, J., Tang, C., and Marius Clore, G. (2007) Practical aspects of ^{1}H transverse paramagnetic relaxation enhancement measurements on macromolecules. *J. Magn. Reson.* **184,** 185–195
47. Delaglio, F., Grzesiek, S., Vuister, G. W., Zhu, G., Pfeifer, J., and Bax, A. (1995) NMRPipe. A multidimensional spectral processing system based on UNIX pipes. *J. Biomol. NMR* **6,** 277–293
48. Johnson, B. A., and Blevins, R. A. (1994) NMR view. A computer program for the visualization and analysis of NMR data. *J. Biomol. NMR* **4,** 603–614
49. Garrett, D. S., Powers, R., Gronenborn, A. M., and Clore, G. M. (1991) A common sense approach to peak picking two-, three- and four-dimensional spectra using automatic computer analysis of contour diagrams. *J. Magn. Reson.* **95,** 214–220
50. Farrow, N. A., Muhandiram, R., Singer, A. U., Pascal, S. M., Kay, C. M., Gish, G., Shoelson, S. E., Pawson, T., Forman-Kay, J. D., and Kay, L. E. (1994) Backbone dynamics of a free and phosphopeptide-complexed Src homology 2 domain studied by ^{15}N NMR relaxation. *Biochemistry* **33,** 5984–6003
51. Iwahara, J., Schwieters, C. D., and Clore, G. M. (2004) Ensemble approach for NMR structure refinement against ^{1}H paramagnetic relaxation enhancement data arising from a flexible paramagnetic group attached to a macromolecule. *J. Am. Chem. Soc.* **126,** 5879–5896
52. Shen, Y., Delaglio, F., Cornilescu, G., and Bax, A. (2009) TALOS^{+}. A hybrid method for predicting protein backbone torsion angles from NMR chemical shifts. *J. Biomol. NMR* **44,** 213–223
53. Ryabov, Y., Schwieters, C. D., and Clore, G. M. (2011) Impact of 15N R2/R1 relaxation restraints on molecular size, shape, and bond vector orientation for NMR protein structure determination with sparse distance restraints. *J. Am. Chem. Soc.* **133,** 6154–6157
54. Xu, C., Gagnon, E., Call, M. E., Schnell, J. R., Schwieters, C. D., Carman, C. V., Chou, J. J., and Wucherpfennig, K. W. (2008) Regulation of T cell receptor activation by dynamic membrane binding of the CD3ϵ cytoplasmic tyrosine-based motif. *Cell* **135,** 702–713
55. Schwieters, C. D., Kuszewski, J. J., Tjandra, N., and Clore, G. M. (2003) The Xplor-NIH NMR molecular structure determination package. *J. Magn. Reson* **160,** 65–73
56. DeLano, W. L. (2002) *The PyMOL Molecular Graphics System*, DeLano Scientific, San Carlos, CA
57. Krueger-Koplin, R. D., Sorgen, P. L., Krueger-Koplin, S. T., Rivera-Torres, I. O., Cahill, S. M., Hicks, D. B., Grinius, L., Krulwich, T. A., and Girvin, M. E. (2004) An evaluation of detergents for NMR structural studies of membrane proteins. *J. Biomol. NMR* **28,** 43–57
58. Bleicken, S., García-Sáez, A. J., Conte, E., and Bordignon, E. (2012) Dynamic interaction of cBid with detergents, liposomes and mitochondria. *PLoS One* **7,** e35910
59. Cho, E. Y., Yun, C. H., and Ahn, T. (2012) Effects of phospholipids on the functional regulation of tBID in membranes. *Mol. Cell Biochem.* **363,** 395–408
60. Katz, C., Zaltsman-Amir, Y., Mostizky, Y., Kollet, N., Gross, A., and Friedler, A. (2012) Molecular basis of the interaction between proapoptotic truncated BID (tBID) protein and mitochondrial carrier homologue 2 (MTCH2) protein. Key players in mitochondrial death pathway. *J. Biol. Chem.* **287,** 15016–15023
61. Zaltsman, Y., Shachnai, L., Yivgi-Ohana, N., Schwarz, M., Maryanovich, M., Houtkooper, R. H., Vaz, F. M., De Leonardis, F., Fiermonte, G., Palmieri, F., Gillissen, B., Daniel, P. T., Jimenez, E., Walsh, S., Koehler, C. M., Roy, S. S., Walter, L., Hajnóczky, G., and Gross, A. (2010) MTCH2/MIMP is a major facilitator of tBID recruitment to mitochondria. *Nat. Cell Biol.* **12,** 553–562
62. Ulmer, T. S., Bax, A., Cole, N. B., and Nussbaum, R. L. (2005) Structure and dynamics of micelle-bound human α-synuclein. *J. Biol. Chem.* **280,** 9595–9603
63. Göbl, C., Dulle, M., Hohlweg, W., Grossauer, J., Falsone, S. F., Glatter, O., and Zangger, K. (2010) Influence of phosphocholine alkyl chain length on peptide-micelle interactions and micellar size and shape. *J. Phys. Chem. B* **114,** 4717–4724
64. Lutter, M., Perkins, G. A., and Wang, X. (2001) The pro-apoptotic Bcl-2 family member tBid localizes to mitochondrial contact sites. *BMC Cell Biol.* **2,** 22
65. Lutter, M., Fang, M., Luo, X., Nishijima, M., Xie, X., and Wang, X. (2000) Cardiolipin provides specificity for targeting of tBid to mitochondria. *Nat. Cell Biol.* **2,** 754–761
66. Kim, T. H., Zhao, Y., Ding, W. X., Shin, J. N., He, X., Seo, Y. W., Chen, J., Rabinowich, H., Amoscato, A. A., and Yin, X. M. (2004) Bid-cardiolipin interaction at mitochondrial contact site contributes to mitochondrial cristae reorganization and cytochrome *c* release. *Mol. Biol. Cell* **15,** 3061–3072
67. Liu, J., Weiss, A., Durrant, D., Chi, N. W., and Lee, R. M. (2004) The cardiolipin-binding domain of Bid affects mitochondrial respiration and enhances cytochrome c release. *Apoptosis* **9,** 533–541
68. Gonzalvez, F., Bessoule, J. J., Rocchiccioli, F., Manon, S., and Petit, P. X. (2005) Role of cardiolipin on tBid and tBid/Bax synergistic effects on yeast mitochondria. *Cell Death Differ* **12,** 659–667
69. Tyurin, V. A., Tyurina, Y. Y., Osipov, A. N., Belikova, N. A., Basova, L. V., Kapralov, A. A., Bayir, H., and Kagan, V. E. (2007) Interactions of cardiolipin and lyso-cardiolipins with cytochrome c and tBid. Conflict or assistance in apoptosis. *Cell Death Differ.* **14,** 872–875
70. Manara, A., Lindsay, J., Marchioretto, M., Astegno, A., Gilmore, A. P., Esposti, M. D., and Crimi, M. (2009) Bid binding to negatively charged phospholipids may not be required for its pro-apoptotic activity *in vivo*. *Biochim. Biophys. Acta* **1791,** 997–1010
71. Gonzalvez, F., Pariselli, F., Jalmar, O., Dupaigne, P., Sureau, F., Dellinger, M., Hendrickson, E. A., Bernard, S., and Petit, P. X. (2010) Mechanistic

issues of the interaction of the hairpin-forming domain of tBid with mitochondrial cardiolipin. *PLoS One* **5,** e9342
72. Petit, P. X., Dupaigne, P., Pariselli, F., Gonzalvez, F., Etienne, F., Rameau, C., and Bernard, S. (2009) Interaction of the α-helical H6 peptide from the pro-apoptotic protein tBid with cardiolipin. *FEBS J.* **276,** 6338–6354
73. Walensky, L. D., Pitter, K., Morash, J., Oh, K. J., Barbuto, S., Fisher, J., Smith, E., Verdine, G. L., and Korsmeyer, S. J. (2006) A stapled BID BH3 helix directly binds and activates BAX. *Mol. Cell* **24,** 199–210
74. Cartron, P. F., Gallenne, T., Bougras, G., Gautier, F., Manero, F., Vusio, P., Meflah, K., Vallette, F. M., and Juin, P. (2004) The first α helix of Bax plays a necessary role in its ligand-induced activation by the BH3-only proteins Bid and PUMA. *Mol. Cell* **16,** 807–818
75. Yethon, J. A., Epand, R. F., Leber, B., Epand, R. M., and Andrews, D. W. (2003) Interaction with a membrane surface triggers a reversible conformational change in Bax normally associated with induction of apoptosis. *J. Biol. Chem.* **278,** 48935–48941
76. Liu, X., Dai, S., Zhu, Y., Marrack, P., and Kappler, J. W. (2003) The structure of a Bcl-xL/Bim fragment complex. Implications for Bim function. *Immunity* **19,** 341–352
77. Yao, Y., Bobkov, A. A., Plesniak, L. A., and Marassi, F. M. (2009) Mapping the interaction of pro-apoptotic tBID with pro-survival BCL-XL. *Biochemistry* **48,** 8704–8711
78. Gavathiotis, E., Suzuki, M., Davis, M. L., Pitter, K., Bird, G. H., Katz, S. G., Tu, H. C., Kim, H., Cheng, E. H., Tjandra, N., and Walensky, L. D. (2008) BAX activation is initiated at a novel interaction site. *Nature* **455,** 1076–1081
79. Czabotar, P. E., Westphal, D., Dewson, G., Ma, S., Hockings, C., Fairlie, W. D., Lee, E. F., Yao, S., Robin, A. Y., Smith, B. J., Huang, D. C., Kluck, R. M., Adams, J. M., and Colman, P. M. (2013) Bax crystal structures reveal how BH_3 domains activate Bax and nucleate its oligomerization to induce apoptosis. *Cell* **152,** 519–531